

A new method for choosing parameters in delay reconstruction-based forecast strategies

Joshua Garland,^{1, a)} Ryan G. James,^{2, b)} and Elizabeth Bradley^{3, c)}

¹⁾ University of Colorado

Department of Computer Science
Boulder, Colorado 80303, USA

²⁾ University of California

Department of Physics, Davis, California 95616, USA

³⁾ University of Colorado

Department of Computer Science, Boulder, Colorado 80303, USA
and the Santa Fe Institute, Santa Fe, New Mexico

ABSTRACT

Delay-coordinate reconstruction is a proven modeling strategy for building effective forecasts of nonlinear time series. The first step in this process is the estimation of good values for two parameters, the time delay and the embedding dimension. Many heuristics and strategies have been proposed in the literature for estimating these values. Few, if any, of these methods were developed with forecasting in mind, however, and their results are not optimal for that purpose. Even so, these heuristics—intended for other applications—are routinely used when building delay coordinate reconstruction-based forecast models. In this paper, we propose a general framework for choosing optimal parameter values for forecast methods that are based on delay-coordinate reconstructions. The basic calculation involves maximizing the shared information between each delay vector and the future state of the system. We illustrate the effectiveness of this method on several synthetic and experimental systems, showing that this way of choosing reconstruction parameters is much more effective than the standard heuristics in the delay-coordinate embedding literature.

I. INTRODUCTION

The method of delays is a well-established technique for reconstructing the state-space dynamics of a system from scalar time-series data^{1–3}. The task of choosing good values for the free parameters in this procedure has been the subject of a large and active body of literature over the past few decades. The majority of these techniques focus on the geometry of the reconstruction. A standard method for selecting the delay τ , for instance, is to maximize independence between the coordinates of the delay vector while minimizing overfitting and reduction in causality between coordinates⁴; a common way to choose an embedding dimension is to track changes in

near-neighbor relationships in reconstructions of different dimensions⁵.

This heavy focus on the geometry of the delay reconstruction is appropriate when one is interested in quantities like fractal dimension and Lyapunov exponents, but it is not necessarily the best approach when one is building a delay reconstruction *for the purposes of prediction*. That issue, which is the focus of this paper, has received comparatively little attention in the extensive literature on delay reconstruction-based prediction^{6–11}. In the following section, we propose a robust, computationally efficient method called SPI that can be used to select parameter values that maximize the shared information between the past and the future—or, equivalently, that maximize the reduction in uncertainty about the future given the current model of the past. The implementation details, and a complexity analysis of the algorithm, are covered in Section III. In Section IV, we show that simple prediction methods working with SPI-optimal reconstructions—constructions using parameter values that follow from the SPI calculations—perform better, on both real and synthetic examples, than those same forecast methods working with reconstructions that are built using the traditional methods mentioned above. Finally, in Section V we explore the behavior of SPI in the face of different data lengths and prediction horizons.

II. SHARED INFORMATION AND DELAY RECONSTRUCTIONS

The information shared between the past and the future is known as the excess entropy¹². We will denote it by $E = I[\overleftarrow{X}; \overrightarrow{X}]$, where I is the mutual information¹³, \overleftarrow{X} represents the infinite past and \overrightarrow{X} the infinite future. E is often difficult to estimate from data due to the need to estimate statistics over potentially infinite random variables¹⁴. While this is possible in principle, it is too difficult in practice for all but the simplest of dynamics¹⁵. In any case, the excess entropy is not exactly what one needs for the purposes of prediction, since it is not realistic to expect to have the infinite past or predict infinitely far into the future. For our purposes, it is more productive to consider the information contained in the

^{a)}Electronic mail: joshua.garland@colorado.edu

^{b)}Electronic mail: rgjames@ucdavis.edu

^{c)}Electronic mail: lizb@colorado.edu

recent past and determine how much that explains about the not-too-distant future. To that end, we define

$$SPI = I[\mathcal{S}_j; X_{j+p}] ,$$

where \mathcal{S}_j is an estimate of the state of the system at time j and X_{j+p} is the state of the system p steps in the future.

This can be neatly visualized—and compared to traditional methods like time-delayed mutual information, multi-information and the so-called co-information¹⁶—using the I-diagrams of Yeung¹³. Figure 1 shows an I-diagram of time-delayed mutual information for a specific τ . In a diagram like this, each circle represents the uncertainty in a particular variable. The left circle in Figure 1, for instance, represents the average uncertainty in observing $X_{j-\tau}$ (i.e., $H[X_{j-\tau}]$, where H is the Shannon entropy¹³); similarly, the top circle represents $H[X_{j+p}]$ or the uncertainty in the p -th future observation. Each of the overlapping regions represents shared uncertainty: e.g., in Figure 1, the shaded region represents the shared uncertainty between X_j and $X_{j-\tau}$. More precisely, the shaded region is

$$\begin{aligned} I[X_j; X_{j-\tau}] &= H[X_j] + H[X_{j-\tau}] - H[X_j, X_{j-\tau}] \\ &= H[X_j] - H[X_j|X_{j-\tau}] \\ &= H[X_{j-\tau}] - H[X_{j-\tau}|X_j]. \end{aligned}$$

If the X are trajectories in reconstructed state space, then tuning the reconstruction parameters (e.g., τ) changes the size of the overlap regions—i.e., the amount of information shared between the coordinates of the delay vector. This notion can be put into practice to select good values for those parameters. Notice, for instance, that minimizing the shaded region in Figure 1—i.e., rendering X_j and $X_{j-\tau}$ as independent as possible—maximizes the total uncertainty that explained by the combined model $[X_j, X_{j-\tau}]^T$ (the sum of the area of the two circles). This is precisely the argument made by Fraser and Swinney in⁴. However, it is easy to see from the I-diagram that choosing τ in this way does not explicitly take into account explanations of the *future*—that is, it does not reduce the uncertainty about X_{t+p} . Moreover, the calculation does not extend to three or more variables, where minimizing overlap is not a trivial extension of the reasoning captured in the I-diagrams.

The obvious next step would be to explicitly include the future in the estimation procedure. One approach to this would be the so-called co-information¹⁶,

$$\mathcal{C} = I[X_j; X_{j-\tau}; X_{j+p}] ,$$

depicted in Figure 2a: the intersection of $H[X_j]$, $H[X_{j-\tau}]$ and $H[X_{j+p}]$. This describes the reduction in uncertainty that the *two* past states, together, provide regarding the future. While this is obviously an improvement over the time-delayed mutual information of Figure 1, it does not take into account the information that is shared between X_j and the future but *not shared with the past* (i.e.,

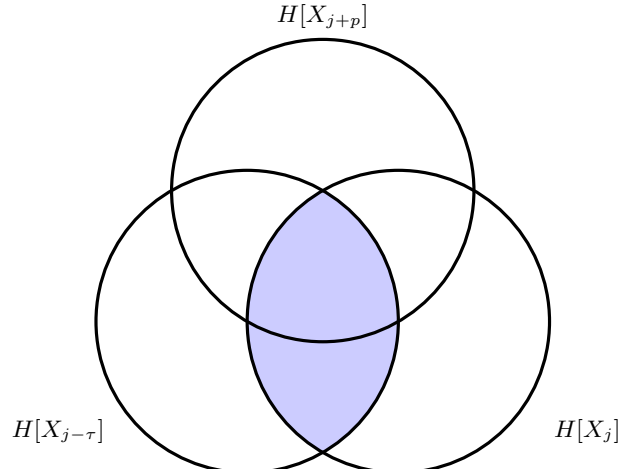


FIG. 1: An I-diagram of the time-delayed mutual information. The circles represent uncertainties (H) in different variables; the shaded region represents $I[X_j; X_{j-\tau}]$, the time-delayed mutual information between the current state X_j and the state τ time units in the past, $X_{j-\tau}$. Notice that the shaded region is indifferent to $H[X_{j+p}]$, the uncertainty about the future.

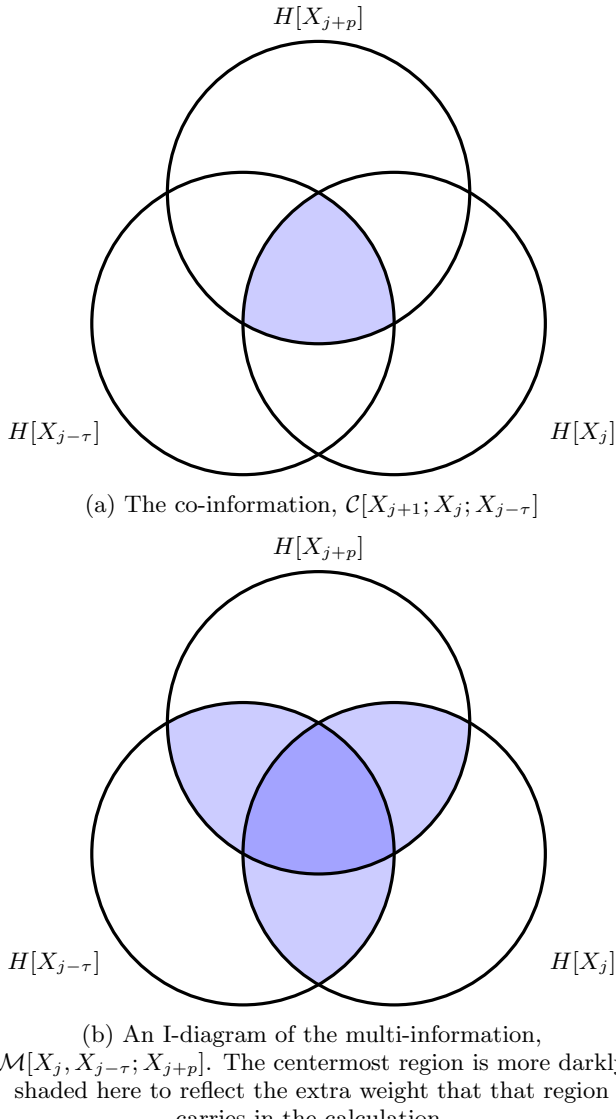
$X_{j-\tau}$), and vice versa. The so-called multi-information

$$\mathcal{M} = \sum_{i \in \{j, j-\tau, j+p\}} (H[X_i]) - H[X_j, X_{j-\tau}, X_{j+p}] ,$$

depicted in Figure 2b addresses this shortcoming, but it also includes information that is shared between the past and the present, but not with the future, which is not useful for the purposes of prediction. Moreover, it overweights information that is shared between all three circles—past, present, and future—which artificially over-values information that is shared in all delay coordinates. In the context of predicting X_{t+p} , the provenance of the information is irrelevant and so the multi-information seems ill-suited to the task at hand as well.

SPI addresses all of the issues raised in the previous paragraphs. By treating the generic delay vector as a joint variable, rather than a series of single variables, SPI captures the shared information between the past, present, and future independently (the left and right colored wedges in Figure 2), as well as the information that the past and present share with the future together (the center wedge). By choosing delay reconstruction parameters that maximize SPI, then, one can explicitly maximize the amount of information that each delay vector contains about the future.

To make all of this more concrete and tie it back to state-space prediction of dynamical systems, consider the following example: let \mathcal{S}_j be a two-dimensional delay reconstruction of the time series, $\mathcal{S}_j = [x_j, x_{j-\tau}]^T$. In this case, SPI becomes $I[[X_j, X_{j-\tau}]^T; X_{t+p}]$, which describes



the reduction in uncertainty about the system at time $j+p$ given the state estimate $[X_j, X_{j-\tau}]^T$. One can estimate a τ for the purposes of reconstructing the dynamics from a given time series, for instance, by calculating SPI for a range of τ and choosing the first maximum (i.e., minimizing the uncertainty about the p -th future observation). One can then apply any state-space forecasting method to the resulting reconstruction in order to predict the future course of that time series. In Section IV, we explore that claim using Lorenz's classic method of analogues¹¹, but it should be just as applicable for other predictors that utilize state-space reconstructions, such as those methods used in^{6-8,10}.

Notice that both the definition of SPI and its use in optimizing forecast algorithms are general ideas that are easily extensible to other state estimators. For example, in the case of traditional delay-coordinate embedding, the

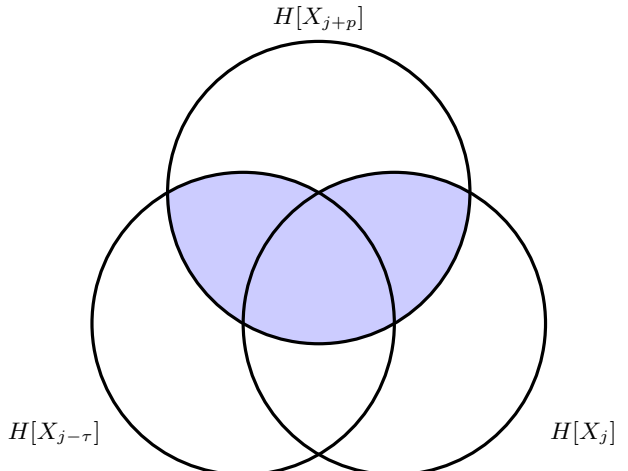


FIG. 2: An I-diagram of SPI, the quantity proposed in this paper: $I[[X_j, X_{j-\tau}]; X_{j+p}]$. This quantity captures the shared information between the past, present, and future independently, as well as the information that the past and present, together, share with the future.

state estimator is the m -dimensional delay vector, i.e.,

$$\mathcal{S}_j = [X_j, X_{j-\tau}, \dots, X_{j-(m-1)\tau}]^T$$

with m chosen to meet various theoretical requirements^{1,3}. We demonstrate this approach in Section IV. If the time series is pre- or post-processed (e.g., via a Kalman filter¹⁷, a low-pass filter and an inverse Fourier transform¹⁸, or some other local linear transformation^{6-8,10,19}), the state estimator simply becomes $\mathcal{S}_j = \hat{x}_j$ where \hat{x}_j is the processed m -dimensional delay vector. As we demonstrate in Section IV B, one can even use SPI to optimize parameter choices for forecast methods that use reconstructions that are not embeddings—i.e., those whose dimensions do not meet the traditional requirements for preserving dynamical invariants like the Lyapunov exponent.

III. EFFICIENT ESTIMATION OF SPI

To calculate SPI from a real-valued time series, one must first symbolize those data. Simple binning is not a good solution here, as is known to cause severe bias if the bin boundaries do not create a generating partition²⁰. A useful alternative is kernel estimation^{21,22}, in which the relevant probability distribution functions are estimated via a function Θ with a resolution or bandwidth r that measures the similarity between two points in $X \times Y$ space. (For SPI, for instance, X would be \mathcal{S}_j and Y would be X_{j+p} .) Given points $\{x_i, y_i\}$ and $\{x'_i, y'_i\}$ in $X \times Y$, one can define:

$$\hat{p}_r(x_i, y_i) = \frac{1}{N} \sum_{i'=1}^N \Theta \left(\left| \begin{array}{c} x_i - x'_i \\ y_i - y'_i \end{array} \right| - r \right) ,$$

where $\Theta(x > 0) = 0$ and $\Theta(x \leq 0) = 1$. That is, $\hat{p}_r(x_i, y_i)$ is the proportion of the N pairs of points in X, Y space that fall within the kernel bandwidth r of $\{x_i, y_i\}$, i.e., the proportion of points similar to $\{x_i, y_i\}$. When $|\cdot|$ is the max norm, this is so-called box kernel. This too, however, can introduce bias²³ and is dependent on the choice of bandwidth r . These estimates, and the analogous estimates for $\hat{p}(x)$, are then used directly to compute local estimates of mutual information for each point in space, which are then averaged over all samples to produce the mutual information of the time series. For more details on this procedure see²³.

A better way to calculate $I[X; Y]$ and estimate SPI is the Kraskov-Stügbauer-Grassberger (KSG) estimator²⁰. This approach dynamically alters the kernel bandwidth to match the density of the data, thereby smoothing out errors in the probability density function estimation process. In this approach, one first finds the k^{th} nearest neighbor for each sample $\{x, y\}$ (using max norms to compute distances in x and y), then sets kernel widths r_x and r_y accordingly and performs the pdf estimation. There are two algorithms for computing $I[X; Y]$ with the KSG estimator²³. The first is more accurate for small sample sizes but more biased; the second is more accurate for larger sample sizes. We use the second of the two in this paper, as we have fairly long time series. In this algorithm, r_x and r_y are set separately, based on x and y distances to the k^{th} nearest neighbor. One then counts the number of neighbors within and on the boundary of these widths in each marginal space, calling these sums n_x and n_y , then calculates

$$I[X; Y] = \psi(k) - \frac{1}{k} - \langle \psi(n_x) + \psi(n_y) \rangle + \psi(n),$$

where ψ is the digamma function. This estimator is bias corrected and has been demonstrated to be robust to variations in k as long as $k \geq 4^{23}$.

In this paper, we employ the Java Information Dynamics Toolkit (JIDT) implementation of the KSG estimator²³. The computational complexity of this implementation is $\mathcal{O}(kN \log N)$, where N is the length of the time series and k is the number of neighbors being used in the estimate. While this is more expensive than traditional binning ($\mathcal{O}(N)$), it is bias corrected, allows for adaptive kernel bandwidth to adjust for under and over sampled regions of space, and is both model and parameter free (aside from k , to which it is very robust).

IV. APPLYING SPI TO SELECT RECONSTRUCTION PARAMETERS

In this section, we provide several examples of how to use SPI to build optimal delay-reconstruction models to be used in forecast methods. We show that the results are identical to those found via exhaustive searches over a range of m and τ . We do this for several synthetic examples as well as on sensor data from several laboratory

experiments. For the discussion that follows, we use the word “optimal” to refer to the set of parameters (m and τ) that provided the lowest forecast error as measured by Mean Absolute Scaled Error ($MASE$)²⁵ over a range of m and τ between the true and predicted signals:

$$MASE = \sum_{j=n+1}^{k+n+1} \frac{|p_j - c_j|}{\frac{k}{n-1} \sum_{i=2}^n |x_i - x_{i-1}|}$$

$MASE$ is a normalized measure: the scaling term in the denominator is the average in-sample forecast error for a random-walk prediction—which uses the previous value in the observed signal as the forecast—calculated over the *initial training signal*, $\{x_j\}_{j=1}^n$ i.e., over the first n elements of the time series. That is, $MASE < 1$ means that the prediction error in question was, on the average, smaller than the in-sample error of a random-walk forecast on the same data. Analogously, $MASE > 1$ means that the corresponding prediction method did *worse*, on average, than the random-walk method. While its comparative nature may seem odd, this error metric allows for fair comparison across varying methods, prediction horizons, and signal scales, making it a standard error measure in the forecasting literature—and a good choice for the study described in the following sections, which involve a number of very different signals.

A. Selecting reconstruction parameters of synthetic time series

In this Section, we apply SPI to several standard synthetic examples: the so-called Lorenz 96 atmospheric model²⁶ and the classic Lorenz 63 model²⁷. For each of these systems, as an initial point of comparison, we approximated the reconstruction parameters through standard heuristics—false-nearest neighbors for m^5 and time-delayed mutual information for τ^4 . As a “best-case” point of comparison we also performed exhaustive search for an optimal forecast parameter over a range of m and τ . ($m = 2, \dots, 15$ and $\tau = 1, \dots, 50$). To this end, we generated 1-step ahead forecasts using Lorenz’s classic method of analogues (LMA)¹¹, which performs basic nearest-neighbor prediction in the reconstructed state space and post facto selecting which parameters were most successful²⁴. Finally, we calculated SPI over the same range of m and τ and selected the $m\text{-}\tau$ set that maximized the resulting SPI surface. We then compared forecast accuracy of each of these methods in Table I and provide the associated reconstruction parameters in Table II. For simplicity, in this initial discussions we set the prediction horizon p to 1. For SPI calculations this means we estimate $I[\mathcal{S}_j, X_{j+1}]$, with $\mathcal{S}_j = [X_j, X_{j-\tau}, \dots, X_{j-(m-1)\tau}]^T$. In Section VB we expand this discussion and consider reaching farther into the future by increasing p . These synthetic examples were integrated with a standard fourth-order Runge-Kutta solver using a timestep of $\frac{1}{64}$ for 60,000 time steps,

the first 10,000 of which were thrown away to remove transient behavior. In this initial discussion we fix all synthetic time series at 50,000 points but we consider the effects of data length in Section V A. We will also apply this method to the Hénon and Logistic Map; two systems which the standard heuristics fail to provide estimates of reconstruction parameters.

Lorenz 96 Atmospheric Model

The Lorenz 96 system²⁶ is defined by a set of K differential equations, $\xi_1 \dots \xi_K$:

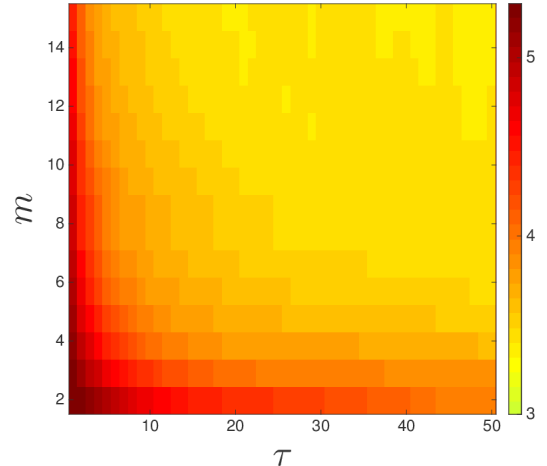
$$\dot{\xi}_k = (\xi_{k+1} - \xi_{k-2})(\xi_{k-1}) - \xi_k + F \quad (1)$$

for $k = 1, \dots, K$, where $F \in \mathbb{R}$ is a constant forcing term that is independent of k . In the following discussion we focus on two parameter sets, $\{K = 22, F = 5\}$ and $\{K = 47, F = 5\}$, these result in low- and high-dimensional chaos respectively. See²⁹ for an explanation of this model and the associated parameters.

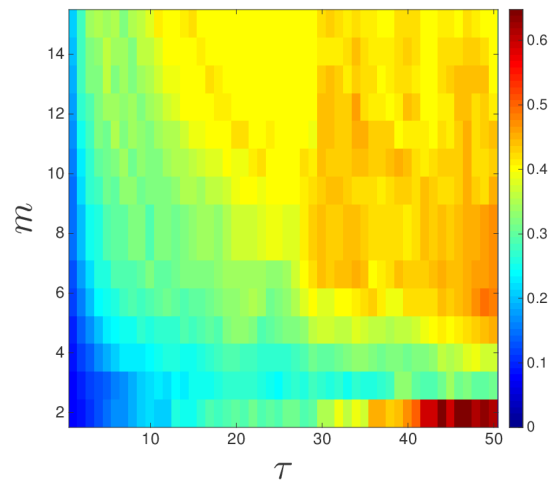
We will begin with discussion using this Lorenz 96 system with $\{K = 22, F = 5\}$. To this end we estimate SPI for a range of m and τ and plotted this in a heat map, seen in Figure 3a. From this map it is clear that there is a strong dependency between the reconstruction parameters m and τ and the reduction in uncertainty about the near future. For example, choosing $m = 2, \tau = 1$ results in a $SPI = 5.303$. If we instead choose m and τ according to standard heuristics^{4,5}, in particular $m = 8, \tau = 26$, this results in $SPI = 3.463$. What this means is that selecting the parameters in the standard fashion results in a significantly less reduction in uncertainty about the future than is possible. This may be counter intuitive. In the standard case you have 6 more dimensions and each delay vector spans much longer distances of the trajectory. It may seem that this would imply each delay vector has more information about the future; What Figure 3a suggests however is that this in fact not the case. As embedding dimension and time delay increase there is a rapid increase in uncertainty about the future. There are several things occurring here including data length, recall here we have fixed data length at 50,000 points—this is discussed further in Section V A and prediction horizon—here we are looking at very short term forecasts—this discussion is expanded in Section V B.

But does this reduction in uncertainty about the future correlate with forecast accuracy of the associated LMA model? Since choosing $m = 2$ and $\tau = 1$ maximizes the shared information between the state estimator and X_{j+1} this would suggest that this selection would minimize 1-step prediction error. To test this we performed an exhaustive search with $m = 2, \dots, 15$ and $\tau = 1, \dots, 50$, and for each m, τ pair we used LMA to generate forecasts and computed the MASE²⁵.

The results of this aforementioned search are shown in Figure 6a. It is another heatmap, but here it is MASE instead of SPI. What is immediately apparent is the



(a) A heatmap of SPI values for Lorenz 96, $\{K = 22, F = 5\}$.



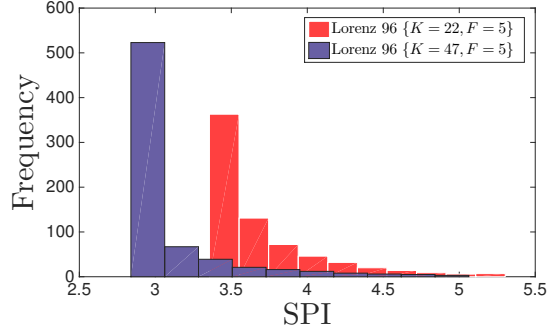
(b) A heatmap of MASE scores for LMA for Lorenz 96, $N = 22, F = 5$.

FIG. 3

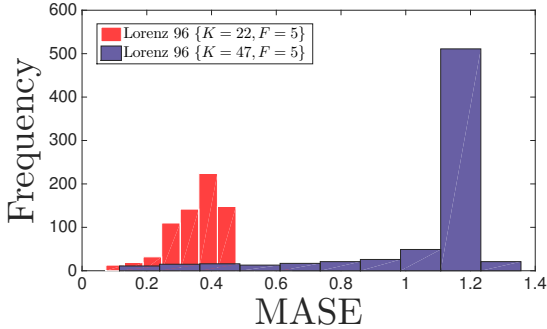
near perfect antisymmetry between this heatmap and the heatmap in Figure 3a. This should make sense: by maximizing the redundancy between the state estimator and the future, we minimize the resulting forecast error of LMA. Indeed, if we choose $m = 2$ and $\tau = 1$ —the maximum of the surface in Figure 3a—we receive a MASE of 0.07373—the minimum of the surface in Figure 6a—compare this to using the standard heuristics^{4,5} which resulted in a MASE of 0.3787. What this illustrates as an initial proof of concept is that SPI lives in almost perfect antisymmetry with forecast error of LMA. This can be leveraged to select forecast specific reconstruction parameters.

If we repeat this experiment but instead use $\{K = 47, F = 5\}$, we receive structurally similar heatmaps to those seen in Figure 3, for this reason they are not shown. Moreover, similar to the $\{K = 22, F = 5\}$ case, minimiz-

ing SPI correctly selected the parameter pair that results in minimal forecast error—and significantly less error than by using standard heuristics, $MASE_{SPI} = 0.1156$ compared to $MASE_H = 1.007$. These results and the associated parameters are tabulated in Tables I and II.



(a) Histograms comparing SPI values for Lorenz 96, $\{K = 22, F = 5\}$ and $\{K = 47, F = 5\}$.



(b) Histograms comparing MASE values for Lorenz 96, $\{K = 22, F = 5\}$ and $\{K = 47, F = 5\}$.

FIG. 4

The main difference in this case is that overall SPI is smaller for nearly all m, τ choices, see Figure 4a. In this figure the blue bars are $K = 47$ and the red bars are $K = 22$. While some of the best-case SPI for $K = 47$ overlap some of the worst case for $K = 22$, in general the $K = 47$ time series has much less information about the future. This is reflected in the resulting forecast accuracy, see Figure 4b. In this Figure the coloring is the same as before and we see that LMA is able to forecast better on $K = 22$ in almost all cases except for a few best-cases overlapping with worst cases scenarios.

Lorenz 63

In Figure 5 we present the same figures as in the previous discussion but constructed using the standard Lorenz

63 model²⁷.

$$\begin{aligned}\dot{x} &= \sigma(y - x), \\ \dot{y} &= x(\rho - z) - y, \\ \dot{z} &= xy - \beta z,\end{aligned}$$

with the typical chaotic parameter selections: $\rho = 28$, $\sigma = 10$, and $\beta = 8/3$.

As was the case with Lorenz 96 in the previous discussion choosing reconstruction parameters using the standard heuristics ($m = 5, \tau = 12$) resulted in significantly less SPI in the associated LMA model (3.348 versus the maximum of 4.5520) and worse forecast accuracy $MASE_H = 0.2215$ as opposed to $MASE_{SPI} = 0.0471$ —a full order of magnitude increase in accuracy! Something interesting to point out in this is that maximizing SPI did not find the optimal minimization of forecast error, but it was close. $MASE_E = 0.04382$ and was associated with a $SPI = 4.518$. The maximal SPI was at 4.552 and resulted in a slightly higher error of $MASE_{SPI} = 0.0471$. This small difference in SPI and MASE show that maximizing SPI may only suggest near-optimal reconstruction parameters due to statistical fluctuation. However, note that maximizing SPI was significantly better than using standard heuristics.

Hénon and Logistic Map

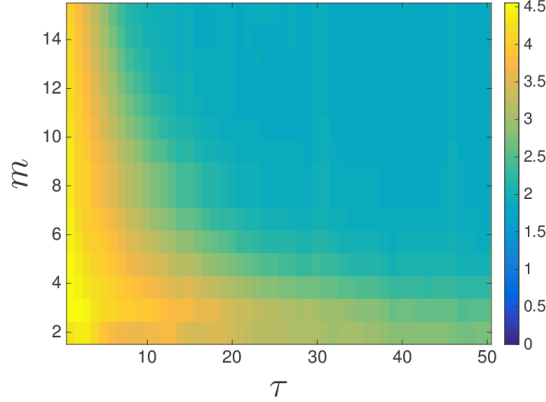
In this section we briefly discuss applying SPI to the Hénon and Logistic Map. These two dynamical systems are interesting examples because delay-coordinate reconstruction should work in theory, however the standard heuristics fail to estimate reconstruction parameters. In particular, for both systems time-delayed mutual information never reaches a minimum, it simply exponentially decays forever. Furthermore, even if one did select a τ , through some other standard method, the mechanics of false-nearest neighbor make no sense in the case of maps. Near-neighbor points that move away from each other need not imply a crossing in the dynamics due to lack of spacial continuity so any of the methods derived from this standard premise would result in a faulty approximation of dimension. As would be the case, even choosing different τ the false-nearest neighbor curve only slowly decreases and never reaches a 10% cut off, even by $m = 15$ —a dimensions far greater than what would be necessary to embed either low-dimensional dynamical system in theory.

For the Hénon map, defined by:

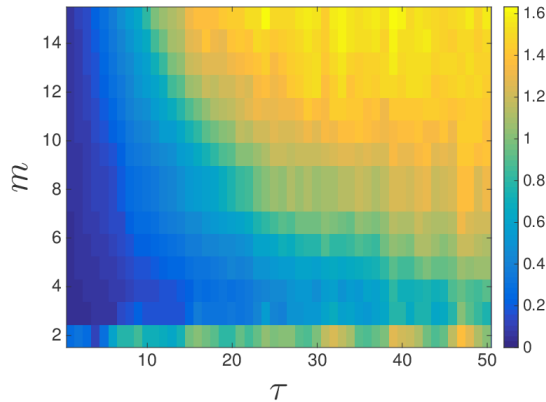
$$x_{n+1} = 1 - ax_n^2 + y_n \quad (2)$$

$$y_{n+1} = bx_n, \quad (3)$$

with $a = 1.4$ and $b = 0.3$, exhaustive search suggested $m = 2, \tau = 1$ would be optimal resulting in $MASE_E = 3.8138 \times 10^{-4}$, a near perfect forecast. These parameters and the associated near perfect forecast make sense. A next-return map of the x -trajectory is effectively the



(a) A heatmap of SPI values for Lorenz 63.



(b) A heatmap of MASE scores for LMA for Lorenz 63.

FIG. 5: SPI vs MASE values for the Lorenz 63 system with standard chaotic parameters, integrated with fourth-order Runge-Kutta using a step size of 0.01.

Hénon map, so by using $[x_j, x_{j-1}]$ as the state estimator you have actually reconstructed the trajectory up to a scaling term. If we follow the procedure above and maximize SPI we do indeed get the same parameter set. So while it is not necessarily interesting that $m = 2, \tau = 1$ are the optimal parameters — these are very obvious from the structure of the map — it is interesting that maximizing SPI allows a practitioner to select this without having this knowledge of the map. Something other standard heuristics are incapable of doing.

Finally, for the Logistic map defined by $x_{n+1} = rx_n(1 - x_n)$ we see again that maximizing SPI selects the optimal reconstruction parameters for forecasting at $m = 1, \tau = 1$, which resulted in another near-perfect forecast: $MASE_E = MASE_{SPI} = 1.6795 \times 10^{-5}$. Again, this choice of parameters makes sense from the form of the map. What is interesting about this finding, is that this suggests for 1-step forecasts of the Logistic Map, *delay-coordinate reconstruction should not be used* instead near-neighbor forecasting on the time series itself

TABLE I: MASE values for various parameter choices. $MASE_H$ is the MASE resulting from standard heuristics. $MASE_{SPI}$ is chosen as the m and τ which maximizes SPI and as a reference $MASE_E$ is exhaustive search to find the minimum error. ** on these signals the standard heuristics failed.

Signal	$MASE_H$	$MASE_{SPI}$	$MASE_E$
Lorenz-96 $K = 22$	0.3787	0.07373	0.07373
Lorenz-96 $K = 47$	1.007	0.1156	0.1156
Lorenz 63	0.2215	0.0471	0.04382
Hénon Map	NA **	3.8138e-04	3.8138e-04
Logistic Map	NA **	1.6795e-05	1.6795e-05

TABLE II: Reconstruction parameter estimates for performing 1-step ahead forecasting. ** on these signals the standard heuristics failed.

Signal	τ_{MI}	m_{FNN}	τ_{SPI}	m_{SPI}	τ_E	m_E
Lorenz-96 $K = 22$	26	8	1	2	1	2
Lorenz-96 $K = 47$	31	10	1	2	1	2
Lorenz 63	12	5	1	3	2	3
Hénon Map	NA **	NA **	1	2	1	2
Logistic Map	NA **	NA **	1	1	1	1

should be performed. Again, something that standard heuristics could not tell you.

Neither of these parameter findings are interesting in and of themselves but this shows a unique feature of SPI. It can be applied to select optimal parameters for forecasting, *even if the system being observed is a map* — something that stymies all the traditional heuristics. It could be argued that selecting these parameters is obvious from the structure of the system, and this is true. However, in the real-world a practitioner is rarely afforded the luxury of knowing this structure. Moreover, maps are commonly observed in practice due to finite sensing and standard heuristics cannot be applied for the above mentioned reasons. However, SPI provides a work around to perform parameter selection in this difficult, important, and often neglected case.

In Tables I and II we tabulate all parameters and errors discussed in this section. In the synthetic case it seems that maximizing SPI minimizes forecast accuracy of LMA. In the next section, we turn our attention to actual experimental time series.

B. Selecting reconstruction parameters of experimental time series

In this section we apply SPI to two experimental time series: measurements of computer performance during the execution of two different programs, and observations from a far-infrared laser.

Computer Performance Dynamics

This experimental example involves data from a laboratory experiment on computer performance dynamics. This system has been shown to exhibit a range of interesting deterministic dynamical behavior, from periodic orbits to low- and high-dimensional chaos^{30,31}, making it a good test case for this paper.

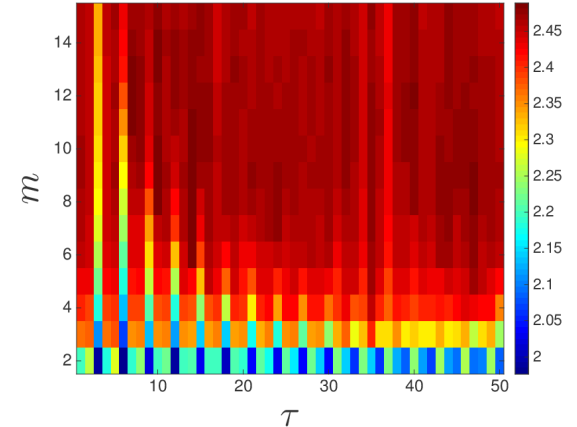
Collecting observations of the performance of a running computer is not trivial. We used the `libpfm4` library, via PAPI (Performance Application Programming Interface) 5.2³², to stop program execution at 100,000-instruction intervals—the unit of time in these experiments—and read the contents of the microprocessor’s onboard hardware performance monitors, which we had programmed to observe important attributes of the system’s dynamics. We leave an in-depth description of this experimental setup to prior works³³. The signals that are produced by this apparatus are scalar time-series measurements of system metrics like processor efficiency (*e.g.*, IPC, which measures how many instructions are being executed, on the average, in each clock cycle) or memory usage (*e.g.*, how often the processor had to access the main memory during the measurement interval).

We have tested this framework on traces of many different processor and memory performance metrics gathered during the execution of a variety of programs on several different computers. Here, for conciseness, we focus on *processor* performance traces from two different programs, one simple and one complex, running on the same Intel i7-based computer. The first is a simple program executing a four-line C program (`col_major`) that repeatedly initializes a 256×256 matrix in column-major order. The second, is the processor efficiency from a much more complex program: the `403.gcc` compiler from the SPEC 2006CPU benchmark suite³⁴.

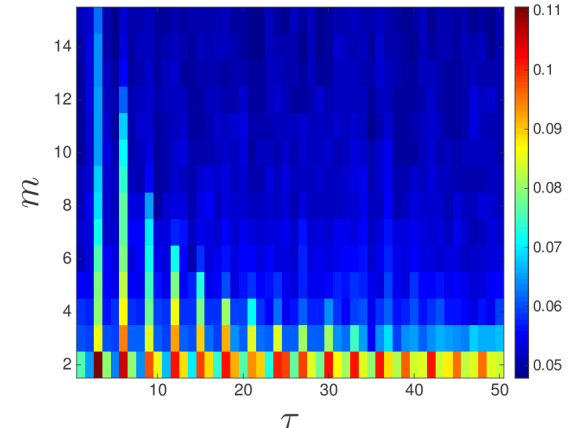
Since computer performance dynamics result from a composition of hardware and software, these two programs represent two different dynamical systems, even though they are running on the same computer.

In Figure 6b we present the same type of heatmaps as before but for the `col_major` experimental time series. As was the case in the synthetic example the two heatmaps are in almost perfect antisymmetry. The oscillatory behavior visible in the bottom left of both plots is easily explained by a dominant unstable periodic orbit of period 3 in the `col_major` dynamics. In this region, any time $\tau = 3k$, $k \in \mathbb{N}$, MASE obtains a local maximum and SPI obtains a local minimum. This is what would

be expected, consider a time series that is actually of period ν then $x_j = x_{j-\nu}$. Now consider choosing $\tau = \nu$: the coordinates of the delay vector are dependent, in fact they are equivalent. It is therefore not surprising that a signal with a strong unstable periodic orbit would be less successful for multiples of that τ as each new coordinate does not provide significant new information. There is a nice theoretical discussion of this in³.



(a) A heatmap of SPI scores for LMA for `col_major`



(b) A heatmap of MASE scores for LMA for `col_major`.

FIG. 6

For the same reasoning it is also not surprising that SPI spikes and MASE plummets at $\tau = 3k - 1$, this is one less than the period of the unstable periodic orbit and so it cannot share any prime factors with the period of the orbit. In this way this choice of τ ensures that each coordinate is not inline with a subharmonic of the period of the orbit and thus each coordinate is in this sense yields the most information. It is also interesting that later multiples, *e.g.*, 6 and 9 actually contain more information than the original period. This corroborates the discussion in³.

What is interesting in this experimental example is

that there is a large set of parameters which are nearly identical statistically in terms of both MASE and SPI, in particular the large dark red/blue regions in Figure 6. All of these parameter choices yield nearly identical SPI and due to the antisymmetry identical MASE. In each of these cases The forecasts are highly accurate 0.05 ± 0.01 , we believe this is due to the signal being nearly periodic. What this type of plot would suggest is that instead of minimizing over m and τ , one should choose an embedding dimension based on algorithmic constraints such as desired near-neighbor search time and then optimize the choice of τ by this measure. For example one might fix $m = 2$ —a technique recently proposed³⁵—because this is computationally the most efficient choice. This would result in a marginalization of the heatmaps in Figure 6. Such a cross section can be seen in Figure 7. Here we again see the antisymmetry and we see that for this fixed m , the choice of τ that minimizes MASE does indeed correspond to the maximal SPI as we would expect.

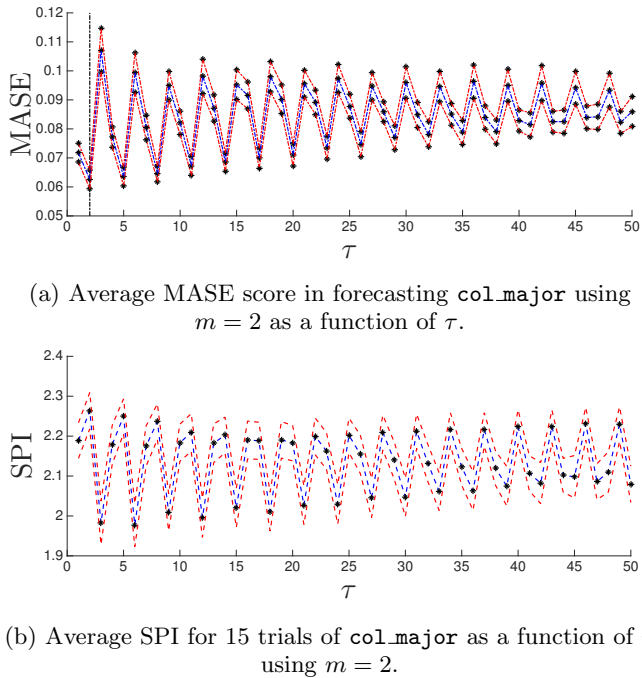


FIG. 7: (a) Average MASE vs τ for LMA forecasts using $m = 2$ for 15 trials of `col_major`. In these figures, the blue dashed curve is the (a) average MASE of these forecasts and (b) the average SPI over 15 trials; the red dotted lines are that average \pm the standard deviation. The black vertical dashed line marks the τ that is the first minimum of the time-delayed mutual information curve for that time series.

Interestingly, in this experimental case using the standard heuristics resulted in the optimal parameter set and as such resulted in a $MASE_H = 0.053$.

`403.gcc` provides a very interesting example. It has been shown in the literature³⁶ that this time series has little to no information sharing with the future, and this

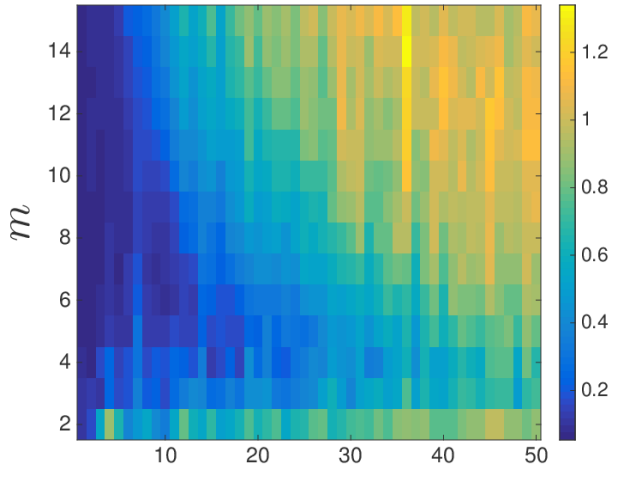
is corroborated with SPI. Averaged over all choices of m and τ , SPI was 0.5730 ± 0.0612 . Compare this to any of the other signals we have examined so far where average SPI is much higher, e.g., 4.5 in the Lorenz 96 $K = 22$ example above. What we would expect from this low SPI and from the previous literature is that regardless of parameter choice LMA would perform poorly on this signal. This is indeed what we see, regardless of parameter choices LMA is unable to forecast lower than a MASE of 1, in fact average MASE was 1.4098 ± 0.0583 . A $MASE > 1$ suggests that a random walk forecast would have out performed the given method, i.e., all LMA methods did worse—significantly worse in some cases—than simply predicting the prior value for the next one. What this suggests is that when SPI is very low for all parameter values another class of forecasting algorithms may be more successful and it may be the case that LMA is not appropriate for any choice of m and τ . See³⁶ for a full discussion of this.

A Far-Infrared Laser

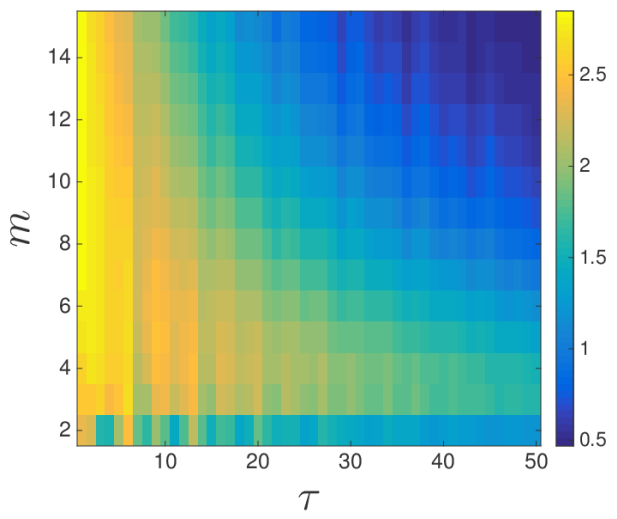
In this section we apply this method to an experimental time series, the so-called “Dataset A”, from a far-infrared laser from the Santa Fe Institute prediction competition⁶. In Figure 8 we again see a great deal of antisymmetry between the SPI and MASE plots. For this experimental data we have a $MASE_H = 0.0733$, which is not that much higher than $MASE_E = 0.0538$ but $MASE_{SPI} = 0.0592$. So in this case the standard heuristics did quite well, but SPI selected a parameter set that was indeed superior. What can be seen from Figure 8 is there are actually a large range of m and τ that have a large SPI value and this corresponds to a wide range of m and τ that also have low MASE. In one of these situations where there is a surface maximum of SPI as opposed to a single point maximum we recommend choosing the smallest m on this surface. This will mitigate noise effects as well as computational burden in the resulting forecast algorithms. In this case, this would mean choosing $m = 4$ and $\tau = 2$ which resulted in a MASE of 0.06351, not optimal but better than $MASE_H$ and uses fewer dimensions. As an aside note the symmetry between Figures 8b and 5. It is well known⁶ that this dataset is well described by the Lorenz 63 system so this symmetry is both unsurprising and reassuring.

V. DATA REQUIREMENT AND PREDICTION HORIZON SPECIFIC PARAMETER ESTIMATION

Thus far in this paper we have fixed the length of our data and the prediction horizon at $p = 1$. In this section we briefly discuss varying these two things and the effects on SPI.



(a) MASE for SFI Dataset A.



(b) SPI for SFI Dataset A.

FIG. 8: The effects of periodicity on SPI.

A. Data Requirements for SPI Estimation

One nice feature of using SPI for parameter selection is that it allows a practitioner to decide how many reconstruction dimensions are appropriate directly from the data that is available. It is common knowledge that the quantity of data used in a delay reconstruction directly impacts the usefulness of the corresponding reconstruction. Unfortunately standard heuristics such as selecting the embedding dimension via false nearest neighbors⁵ often do not take into account how much data is necessary to fill out the suggested dimension. There do exist bounds on how much data is needed for a given dimension^{37,38}, however, these bounds directly depend

on the application of the reconstruction. For example, the bounds in³⁷ were derived for the specific purposes of approximating the correlation dimension via the Grassberger-Procaccia algorithm; in our opinion, they are overly pessimistic for forecasting. Often successful forecasting can be accomplished with orders of magnitude less data than these bounds would suggest. For example, Sugihara & May¹⁰ used delay-coordinate embedding with m as large as seven to successfully forecast biological and epidemiological time-series data as short as 266 points!

When choosing reconstruction parameters using SPI you allow the amount of data present to dictate what dimension to use. When data lengths are small low-dimensional reconstructions that do not satisfy the associated embedding theorems seem to be more successful than utilizing the “correct” parameters in spite of not having the quantity of data to justify it. This makes perfect sense. When an ill-sampled high-dimensional manifold is projected onto a low dimensional space, ill-sampled regions or regions that are not visited frequently in the high-dimensional space can act effectively like noise in the reconstruction space. From an information-theoretic standpoint this would increase the effective Shannon entropy rate of each of the variables in the reconstruction vector. In the I-diagram in Figure 2 this would be equivalent to each of the circles drifting apart, which in turn decreases the shaded region that we need to maximize for effective forecasting. One way of testing this in the synthetic case would be to increase data length and rerun the experiment. Viewing the problem from this point of view, the increase in data length would (hopefully) fill out areas of the high-dimensional space and mitigate the spurious increase in the Shannon entropy rate. As more data becomes available it may become the case that a higher dimensional embedding will be more effective since the higher dimensional spaces have the data to begin to fill out. As we will show, this type of analysis can be done directly from the time series using SPI and no theoretical bounds on dimensionality are necessary.

To test this hypothesis we increased the length of the observations of the two synthetic examples²⁸ and test whether the information content of the state estimator derived from standard heuristics gets closer to the SPI-optimal estimator. In Figure 9 we have increased Lorenz 96 (a) $K = 22, F = 5$ and (b) $K = 47, F = 5$, time series from 500 to 4 million points and calculated SPI for the optimal τ (as determined by SPI) value ($\tau = 1$) for $m = 2, 4$ and 8 over 15 different trajectories.

In both panels of Figure 9 blue corresponds to $m = 2$, purple to $m = 4$ and red to $m = 8$. In both cases for small data length the $m = 2$ state estimator had the most information about the future. This echoes earlier observations as there is not enough data to fill out the higher-dimensional reconstructions. As data increases however the higher-dimensional reconstructions get more information about the future as the space fills out. In both cases once the training signal is 2 million points long

the $m = 4$ state estimator has caught up to and even succeeded the SPI in the two-dimensional case. In both cases, the $m = 8$ embedding does not catch up to either the $m = 2$ or 4 reconstruction. This means that even if the time series were 4 million points long for either of these systems, using a lower dimensional reconstruction is more effective based on information about the future.

Something very interesting happens to the $m = 2$ results for Lorenz 96 model with $K = 47$. The curve reaches a maximum value and stops increasing regardless of data length. What this means is that once the two-dimensional model has 100,000 points (for this time series) it has all the information that it can ascertain about the next-step future no matter how many points are added. In other words keeping around 1 million points or 100,000 points you would expect the exact same forecasting performance and this is in fact the case. After 100,000 points LMA with $m = 2$ had approximately 5.736 SPI and 0.0809 MASE. This was tested for 15 trajectories of length 100,000, 1 million and 2.2 million. Due to this plateau behavior $m = 4$ is able to surpass $m = 2$ at around 2 million points and as data continues to grow in length the 4 dimensional reconstruction grows in SPI. What this suggests is that for most forecasts using a training set larger than 2.5 million data points then $m = 4$ would provide a slightly more accurate forecast (MASE of 0.0521) albeit at the cost of keeping in memory an additional 2 dimensions, which could in fact be a significant problem with training sets that long; particularly considering that almost the exact same performance is possible using only 100,000 points and $m = 2$. In neither case did $m = 8$ catch up to either $m = 2$ or $m = 4$ even at 4 million data points. This suggests that even with 4 million data points you are still better off using a low-dimensional reconstruction.

B. Choosing reconstruction parameters for increased prediction horizons.

So far in this paper we have exclusively considered short-term forecasts, i.e. $I[\mathcal{S}_j, X_{j+1}]$. In this section we extend this conversation to longer prediction horizons using $I[\mathcal{S}_j, X_{j+p}]$, with $p > 1$. Of course as we need to reach farther into the future, it is not surprising that the best reconstruction dimension and time delay may change. For example, it may be the case that one needs to reach different distances into the past to reduce the uncertainty about farther events into the future, whereas short term forecasts generally do better with small tau. This effect has been seen in the literature^{19,35} and is corroborated by SPI.

In Figure 10 we consider the Lorenz 96 model with $K = 22$ and plot the average SPI as a function of τ , fixing $m = 2$ for simplicity, over several different prediction horizons. The top most line is $p = 1$, the second is $p = 2$ and so on all the way to the bottom most line which is $p = 100$. A few things to note is that as prediction

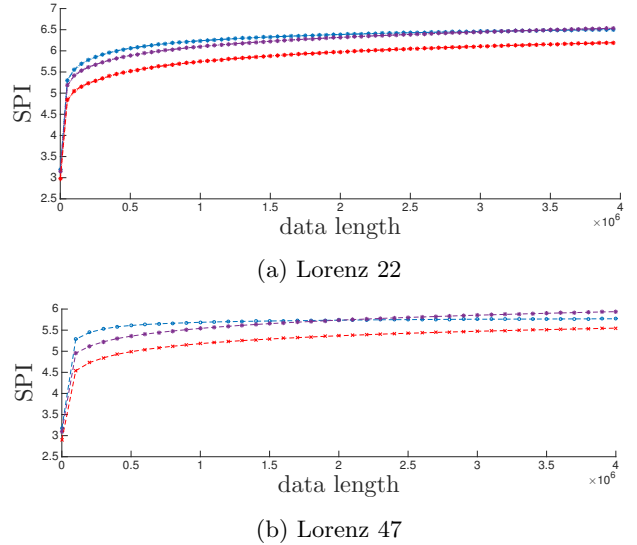


FIG. 9: The values of SPI versus data length for the two Lorenz 96 models. Blue data corresponds to an embedding dimension $m = 2$, purple to $m = 4$, and red to $m = 8$.

horizon increases (going down the plot) the optimal τ shifts to the right, i.e., longer prediction horizons require a greater τ , cf.¹⁹. Also notice that for very long prediction horizons the choice of τ should matter very little. There is almost no difference in SPI between $\tau = 5$ and 50 for p greater than 30. We believe at this point LMA will perform poorly regardless of the choice of τ . This is because SPI is now one third of what it was for $p = 1$, i.e., there is three times less reduction in uncertainty about the future for p greater than 30. This is not a surprising result, and indeed is suggested in the literature, but something to keep in mind when predicting over different prediction horizons: it may be that the optimal choice of reconstruction parameters change. Fortunately SPI can quantify when this is the case.

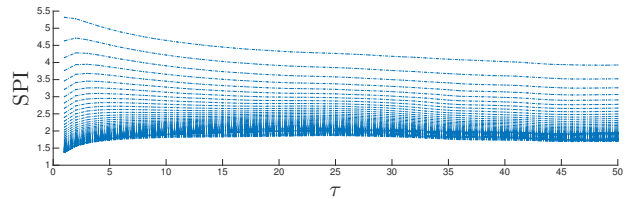


FIG. 10: The effect of prediction horizon on optimal τ for a fixed reconstruction dimension ($m = 2$). The system considered here is the Lorenz 96 model with $K = 22$. The lines, starting from the top, correspond to prediction horizons of $p = 1$ to $p = 100$.

Just as τ may change with increasing prediction horizon, the same is the case with reconstruction dimension. As forecasts horizons grow increasing the reconstruction dimension can—depending on available data—allow for

more memory about the past which effectively gives you more information—in most cases—about the future⁶.

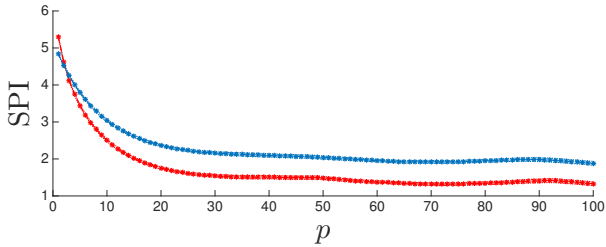


FIG. 11: The effect of prediction horizon on SPI for the Lorenz 96 with $K = 22$. Here, τ is fixed at 1, and we consider two values of m : the red line is $m = 2$ and the blue is the standard LMA, where m is selected via the false nearest neighbors technique.

Figure 11 shows curves of SPI as a function of prediction horizon for fixed $\tau = 1$ and two different m , the red curves are $m = 2$ and the blue curves are the m selected by the standard heuristic. There are a few features of this plot to notice. To begin, both curves are monotonically decreasing with prediction horizon. This is what we would suspect using a near-neighbor forecasting scheme on a system with a positive Lyapunov exponent: Pesin's relation⁴⁰ says that the sum of the positive Lyapunov exponents is equal to the entropy rate, and if there is a non-zero entropy rate, then generically observations will become increasingly independent the further apart they are. If the signal were nearly periodic (heavily influenced by a dominant UPO) this would not be the case as demonstrated in Figure 12. Also notice the $m = 2$ state estimator loses information about the future faster than the full reconstruction. This can be seen by the initial drop being more drastic in the $m = 2$ case. For the Lorenz 96 $K = 22$ case, Figure 11, this allowed the full reconstruction to begin forecasting more accurately as the higher reconstruction dimension retained more information about the future for longer. So while $m = 2$ does better for short prediction horizons it will begin to do worse than the standard method as prediction horizon increases. This is exactly what we see with the p -MASE scores as well.

Figure 12 is interesting because the `col_major` signal is very near an unstable periodic orbit. When using $m = 2$, we see that SPI is consistently has less than the full reconstruction for all prediction horizons, which is what one might expect due to the strong period-3 component in the signal. The jagged behavior in the $m = 2$ case can be explained by considering the unstable period orbit. The peaks of these oscillations occur at every multiple of three, meaning $m = 2$ state estimator can forecast with the most success when the value being predicted is in-phase with the delay vector. As expected, the SPI function decays over time initially but interestingly begins to rise again and peaks at $p = 69$ and $p = 71$. We believe this suggests that `col_major` may also have a higher-

order unstable periodic orbit. This analysis suggests that when forecasting nearly periodic signals, the SPI is maximized when p is in phase with the UPO and while τ is out of phase.

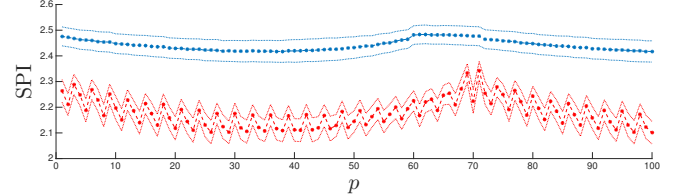


FIG. 12: The effect of prediction horizon on SPI for `col_major`. Here, τ is fixed at the SPI-optimal values for $p = 1$, and we consider two values of m : the red line is $m = 2$ and the blue line has m selected via the false nearest neighbors technique on the `col_major` signal.

In theory we can derive rigorous bounds on prediction horizon. The time at which \mathcal{S}_j will no longer have any information about the future can be determined by considering:

$$R(p) = \frac{I[\mathcal{S}_j; X_{j+p}]}{H[X_{j+p}]} ,$$

the percentage of the uncertainty in X_{j+p} which can be reduced by the delay vector. Generically, this will limit to some small value equal to the amount of information the delay vector has about any arbitrary point on the attractor. Using the behavior of this curve, one can select a maximum horizon based on some criteria regarding how much information above the “background” they would like their predictor to have.

By explicitly including forecast horizon in the SPI function we can select optimal or near-optimal parameters for a given forecast horizon by fixing p at the required forecast horizon and performing the same search as we did in earlier sections over a range of m and τ finding a point or surface of parameters which maximize SPI for that particular forecast horizon. Something other heuristics are incapable of doing.

VI. CONCLUSION

In this paper we have developed a general framework that quantifies the reduction in uncertainty about the future for any LMA-based model being used for forecasting, regardless of the choice of state estimator. Using this framework we answered many questions regarding forecasting using theoretically unsound models³⁵, including but not limited to τ selection. In particular, SPI allows one to select τ in an optimal forecasting sense, without performing an exhaustive search. Additionally, SPI allows for direct comparison between different parameter selection methods, and suggests which will be the most appropriate based on several considerations e.g.,

data length, signal and forecast horizon. SPI also allows one to better understand bounds on prediction horizon without the need to estimate Lyapunov spectra or Shannon entropy rates, which are both the traditional methods and useful in theory, but are difficult to obtain for arbitrary real-valued time series. Finally, SPI provides a measure to perform model selection based on constraints such as data length and prediction horizon needs. This framework is general and easily extensible to more advanced near-neighbor delay-coordinate embedding techniques such as those used in^{6–8,10,18}.

SPI can be used to select both m and τ simultaneously: simply choose $\mathcal{S}_j = [X_j, X_{j-\tau}, \dots, X_{j-(m-1)\tau}]$ for a range of m and τ and select the (m, τ) that maximizes this surface. This can be done with deference to data length and prediction horizon, without needing to know such quantities as the Lyapunov exponents, governing equations or dimension of the time series. While this work focused on results specifically about unfiltered delay vectors, we have shown that our method is applicable to pre- and/or post-processes delay vectors by substituting the state estimator for a filtered delay vector.

The framework presented here is very general and has quite a bit of room for extension or adaptation for domain-specific concerns. As a result there are many interesting future directions for this research. Since there is no particular reason that the delays all be equal, one such direction is using SPI to adapt τ for each dimension. In particular, one could define $\mathcal{S}_j = [X_j, X_{j-\tau_1}, X_{j-\tau_2}, \dots, X_{j-\tau_{m-1}}]$ and then simply maximize SPI using that state estimator constrained over $\{\tau_i\}_{i=1}^{m-2}$. Another not so obvious extension is to use SPI to inform a practitioner about sampling rate. If SPI is optimized with $\tau = 1$, this perhaps suggests that the sampling rate should be increased, where as if $\tau = 1000$ maximizes SPI then maybe not as much sampling is necessary as informative samples are quite distant.

VII. REFERENCES

- ¹F. Takens, Detecting strange attractors in fluid turbulence, in: D. Rand, L.-S. Young (Eds.), *Dynamical Systems and Turbulence*, Springer, Berlin, 1981, pp. 366–381.
- ²N. Packard, J. Crutchfield, J. Farmer, R. Shaw, Geometry from a time series, *Physical Review Letters* 45 (1980) 712.
- ³T. Sauer, J. Yorke, M. Casdagli, Embedology, *Journal of Statistical Physics* 65 (1991) 579–616.
- ⁴A. Fraser, H. Swinney, Independent coordinates for strange attractors from mutual information, *Physical Review A* 33 (2) (1986) 1134–1140.
- ⁵M. Kennel, R. Brown, H. Abarbanel, Determining minimum embedding dimension using a geometrical construction, *Physical Review A* 45 (1992) 3403–3411.
- ⁶A. Weigend, N. Gershenfeld (Eds.), *Time Series Prediction: Forecasting the Future and Understanding the Past*, Santa Fe Institute Studies in the Sciences of Complexity, Santa Fe, NM, 1993.
- ⁷M. Casdagli, S. Eubank (Eds.), *Nonlinear Modeling and Forecasting*, Addison Wesley, 1992.
- ⁸L. Smith, Identification and prediction of low dimensional dynamics, *Physica D: Nonlinear Phenomena* 58 (1–4) (1992) 50 – 76.
- ⁹A. Pikovsky, Noise filtering in the discrete time dynamical systems, *Soviet Journal of Communications Technology and Electronics* 31 (5) (1986) 911–914.
- ¹⁰G. Sugihara, R. May, Nonlinear forecasting as a way of distinguishing chaos from measurement error in time series, *Nature* 344 (1990) 734–741.
- ¹¹E. Lorenz, Atmospheric predictability as revealed by naturally occurring analogues, *Journal of the Atmospheric Sciences* 26 (1969) 636–646.
- ¹²J. P. Crutchfield, D. P. Feldman, Regularities unseen, randomness observed: Levels of entropy convergence, *Chaos: An Interdisciplinary Journal of Nonlinear Science* 13 (1) (2003) 25–54.
- ¹³R. W. Yeung, *A first course in information theory*, Springer Science & Business Media, 2012.
- ¹⁴R. G. James, J. R. Mahoney, C. J. Ellison, J. P. Crutchfield, Many roads to synchrony: Natural time scales and their algorithms, *Physical Review E* 89 (4) (2014) 042135.
- ¹⁵C. C. Strelcoff, J. P. Crutchfield, Bayesian structural inference for hidden processes, *Physical Review E* 89 (4) (2014) 042119.
- ¹⁶A. J. Bell, The co-information lattice, in: *Proceedings of 4th International Symposium on Independent Component Analysis and Blind Source Separation*, 2003, pp. 921–926.
- ¹⁷H. W. Sorenson, *Kalman Filtering: Theory and Application*, IEEE Press, 1985.
- ¹⁸T. Sauer, Time-series prediction by using delay-coordinate embedding, in: *Time Series Prediction: Forecasting the Future and Understanding the Past*, Santa Fe Institute Studies in the Sciences of Complexity, Santa Fe, NM, 1993.
- ¹⁹H. Kantz, T. Schreiber, *Nonlinear Time Series Analysis*, Cambridge University Press, Cambridge, 1997.
- ²⁰A. Kraskov, H. Stögbauer, P. Grassberger, Estimating mutual information, *Physical review E* 69 (6) (2004) 066138.
- ²¹T. Schreiber, Measuring information transfer, *Phys. Rev. Lett.* 85 (2000) 461–464. doi:10.1103/PhysRevLett.85.461.
- ²²S. Frenzel, B. Pompe, Partial mutual information for coupling analysis of multivariate time series, *Phys. Rev. Lett.* 99 (2007) 204101. doi:10.1103/PhysRevLett.99.204101.
- ²³J. T. Lizier, Jidt: An information-theoretic toolkit for studying the dynamics of complex systems, *Frontiers in Robotics and AI* 1 (11).
- ²⁴Maybe add a sentence about how algorithm 1 differs from this?
- ²⁵R. Hyndman, A. Koehler, Another look at measures of forecast accuracy, *International Journal of Forecasting* 22 (4) (2006) 679–688.
- ²⁶E. Lorenz, Predictability: A problem partly solved, in: T. Palmer, R. Hagedorn (Eds.), *Predictability of Weather and Climate*, Cambridge University Press, 2006, pp. 40–58.
- ²⁷E. Lorenz, Deterministic nonperiodic flow, *Journal of the Atmospheric Sciences* 20 (1963) 130–141.
- ²⁸This is not possible in practice, but provides for a nice comparison.
- ²⁹A. Karimi, M. Paul, Extensive chaos in the Lorenz-96 model, *Chaos: An Interdisciplinary Journal of Nonlinear Science* 20 (4).
- ³⁰Z. Alexander, T. Mytkowicz, A. Diwan, E. Bradley, Measurement and dynamical analysis of computer performance data, in: *Proceedings of Advances in Intelligent Data Analysis IX*, Vol. 6065, Springer Lecture Notes in Computer Science, 2010.
- ³¹T. Mytkowicz, A. Diwan, E. Bradley, Computers are dynamical systems, *Chaos: An Interdisciplinary Journal of Nonlinear Science* 19 (3).
- ³²S. Browne, C. Deane, G. Ho, P. Mucci, PAPI: A portable interface to hardware performance counters, in: *Proceedings of Department of Defense HPCMP Users Group Conference*, 1999.
- ³³T. Mytkowicz, Supporting experiments in computer systems research, Ph.D. thesis, University of Colorado (November 2010).
- ³⁴J. Henning, SPEC CPU2006 benchmark descriptions, *SIGARCH Computer Architecture News* 34 (4) (2006) 1–17.
- ³⁵J. Garland, E. Bradley, Prediction in projection, in review at

CHAOS; Preprint available at arXiv:1503.01678. (2015).

³⁶J. Garland, R. James, E. Bradley, Model-free quantification of time-series predictability, *Physical Review E* 90 (2014) 052910.

³⁷A. A. Tsonis, J. B. Elsner, K. P. Georgakakos, Estimating the dimension of weather and climate attractors: Important issues about the procedure and interpretation, *Journal of the Atmospheric Sciences* 50 (15) (1993) 2549–2555.

³⁸L. Smith, Intrinsic limits on dimension calculations, *Physical Letters A* 133 (6) (1988) 283–288.

³⁹This is not possible in practice but can be done in this synthetic setting.

⁴⁰Y. B. Pesin, Characteristic lyapunov exponents and smooth ergodic theory, *Russian Mathematical Surveys* 32 (4) (1977) 55–114.